Supplementary Information (SI) for Journal of Materials Chemistry A.

Radiation Hardness Analysis of 2D Layered Perovskite Photovoltaics in the Space Environment

Mustafa Kareem[1,*], Bassam Thaban[1]

[1]College of Remote Sensing and Geophysics, Al-Karkh University of Science, Haifa St., Baghdad 10011, Iraq

***Corresponding author email:** dr.mustafa@kus.edu.iq

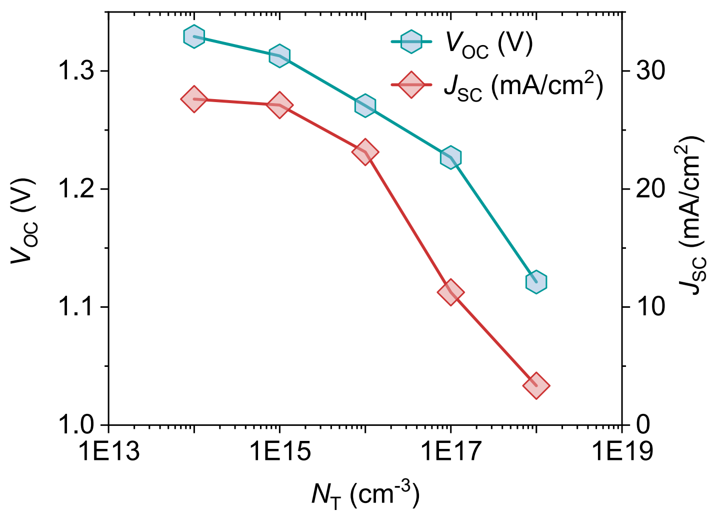

Figure S1: Influence of perovskite trap-state density (N_T) on the V_{OC} and J_{SC}.

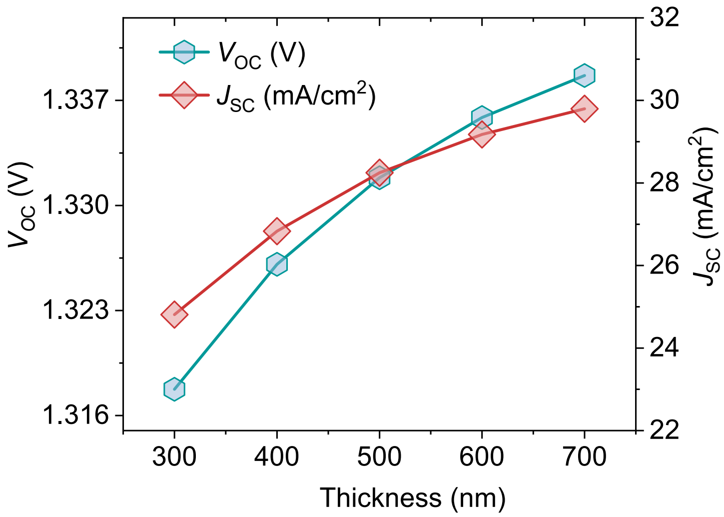

Figure S2: Influence of perovskite layer thickness on the V_{OC} and J_{SC}.

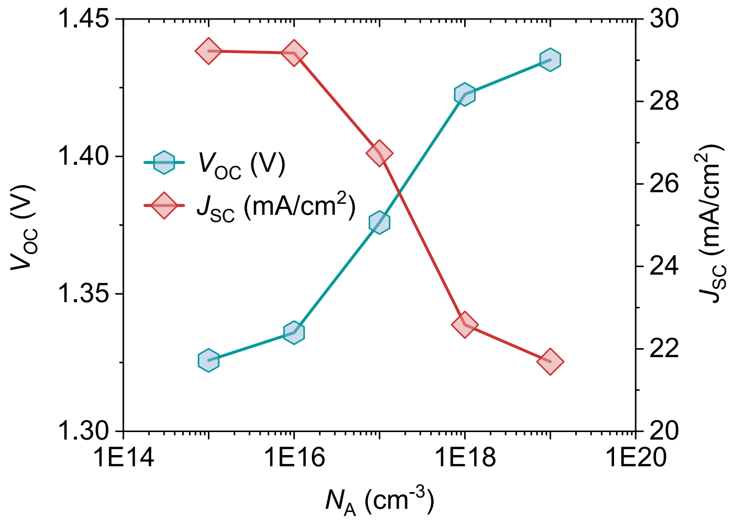

Figure S3: Influence of perovskite shallow acceptor concentration (N_A) on the V_{OC} and J_{SC}.

Discussion:

Figure S4a shows the *J-V* curves of PSCs at different N_A levels in the graphene layer. The N_A doping is adjusted between 10^{15} and 10^{19} cm^{-3}, while maintaining a constant N_D doping of the MoS_2 layer. As depicted in Figures **S4b** and **S4c**, all device parameters improve with increasing doping level of graphene. The simulated devices showed enhanced IPCE spectra in the visible light spectrum, indicating favorable hole extraction at the perovskite/graphene interface (**Figure S4d**). Additionally, FF showed significant enhancement due to reducing charge-carrier accumulation and improving R_{rec}, facilitating charge transport, as proven by **Figures S4e**. The champion PSCs attained a high PCE of 20.37% with a V_{OC} of 1.37 V at a N_A of 10^{19} cm^{-3}. Similarly, the shallow donor doping (N_D) in MoS_2 is altered from 10^{15} to 10^{19} cm^{-3}, while keeping a fixed N_A doping of the graphene film at 10^{19} cm^{-3}. As shown in **Figures S4f-h**, the donor doping is mostly improving FF and PCE, while V_{OC} and J_{SC} showed stable patterns. According to **Figure S4i**, devices with high N_D levels have the largest semi-circular arcs of R_{rec}, which gives evidence of mitigated trap-assisted recombination sites and improved charge transfer. The optimized fully 2D PSC obtained an efficiency of 20.92% with a FF of 70.55%, a V_{OC} of 1.37 V, and a J_{SC} of 29.24 mA/cm^2.

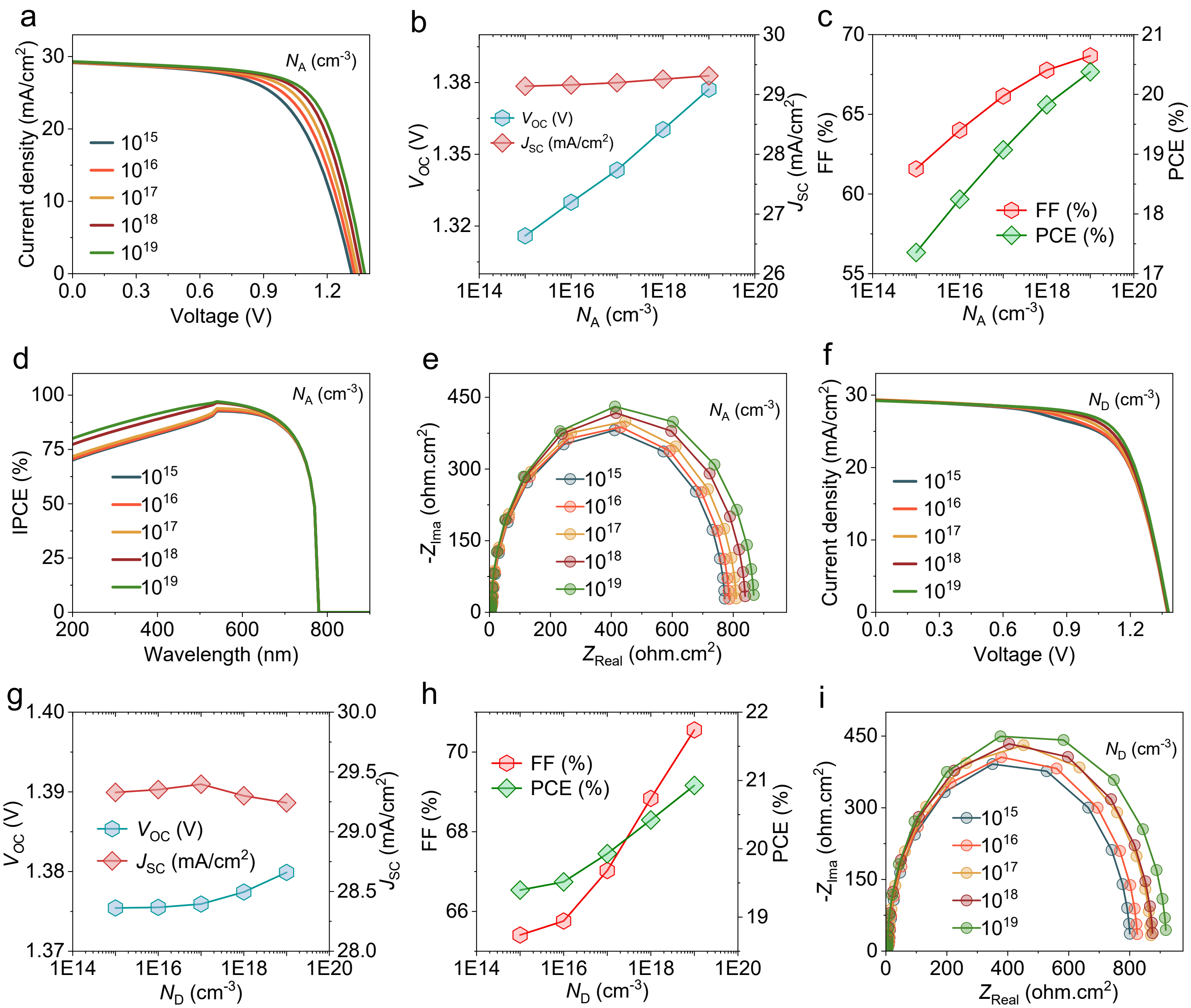

Figure S4: SCAPS-1D simulation results for fully 2D PSCs under varied doping concentrations in MoS_2 and graphene layers. **(a)** *J–V* curves at different shallow acceptor density (N_A) of graphene. **(b)** Corresponding V_{OC} and J_{SC} variation with N_A. **(c)** FF and PCE responses versus N_A. **(d)** N_A-dependent variation of IPCE spectrum. **(e)** Nyquist plots. **(f)** *J–V* curves at different shallow donor density (N_D) of MoS_2. **(g)** Corresponding V_{OC} and J_{SC} variation with N_D. **(h)** FF and PCE responses versus N_D. **(i)** Nyquist plots.

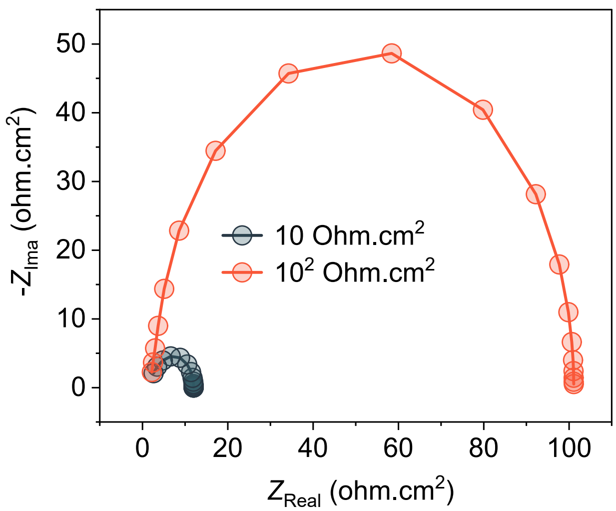

Figure S5: Nyquist plots of 2D PSCs at 10 and 10^2 Ohm.cm^2 shunt resistances.

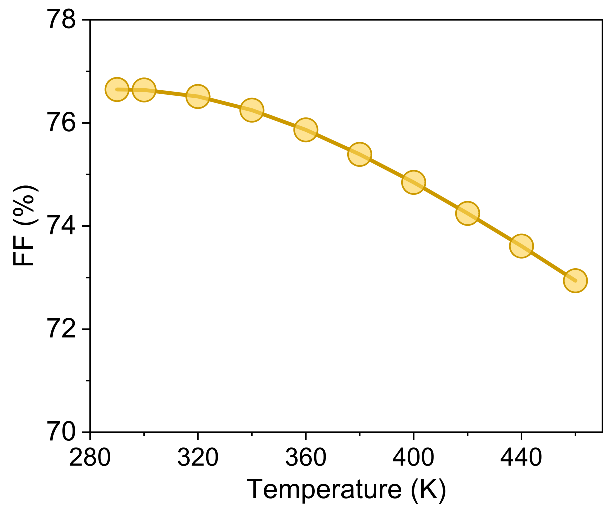

Figure S6: Temperature-dependent FF of 2D PSC.

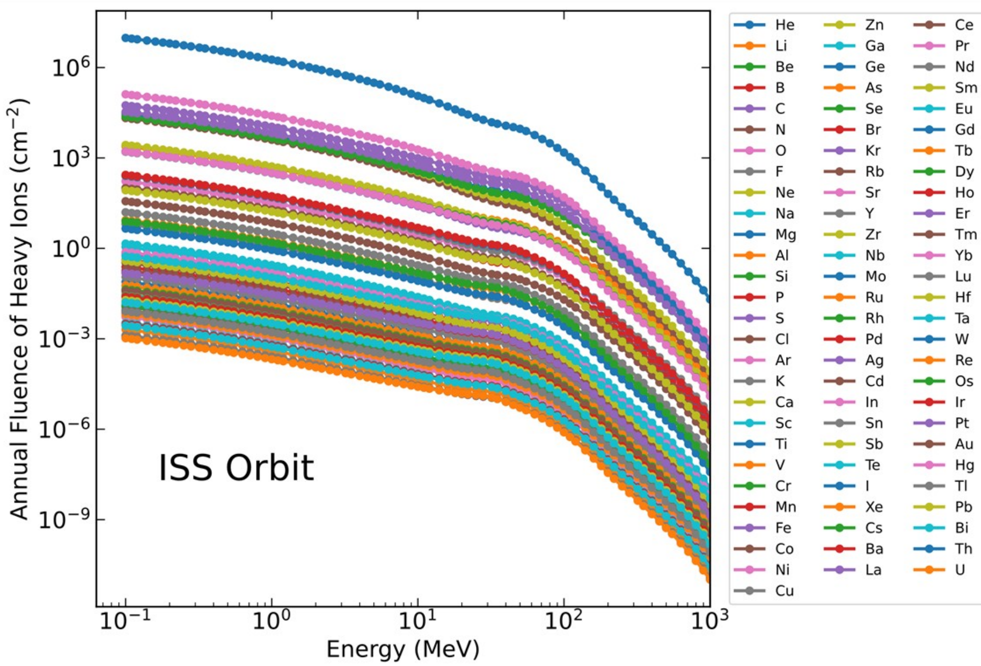

Figure S7: Annual fluence of heavy ions as a function of particle energy in the ISS orbit.

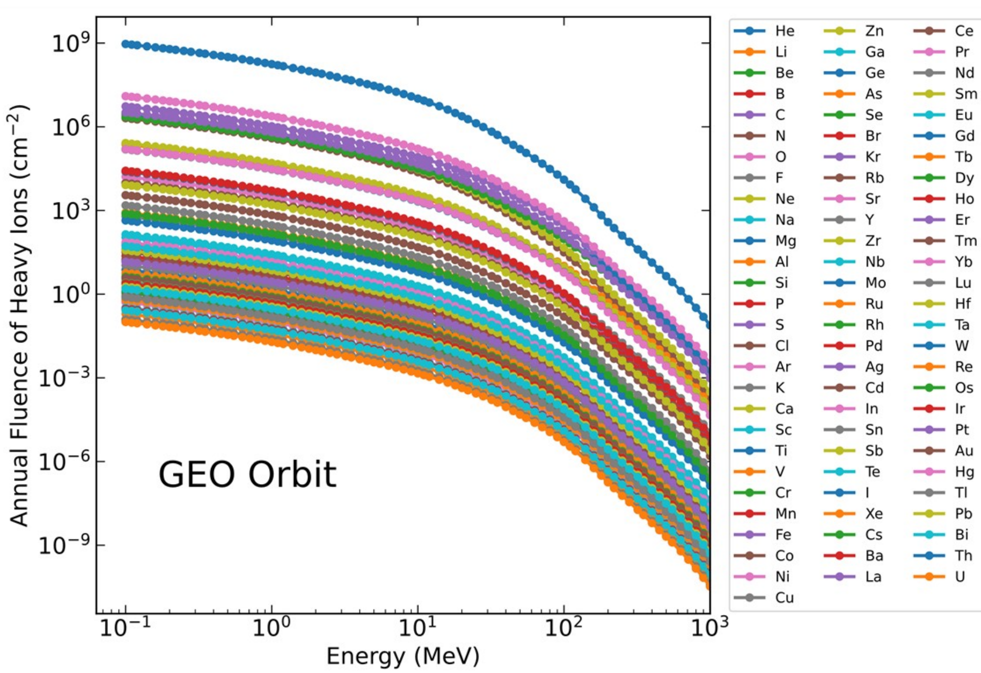

Figure S8: Annual fluence of heavy ions as a function of particle energy in the GEO orbit.

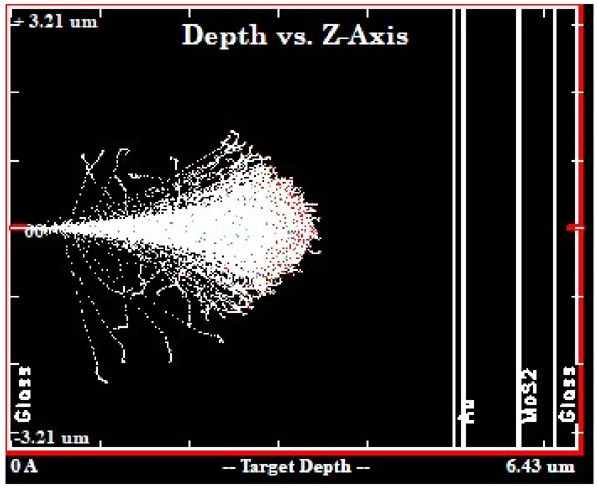

Figure S9: Proton straggling within the protected device at θ = 0^o and 0.25 MeV.

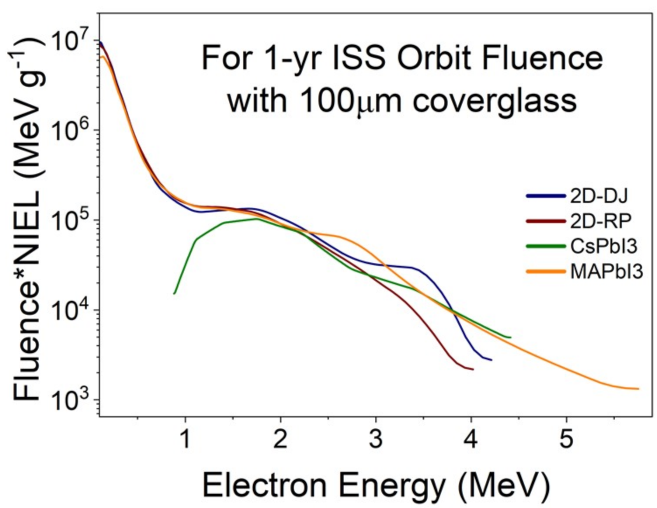

Figure S10. Displacement damage dose (DDD) versus electron energy for the ISS orbit, computed from one-year electron fluence, with a 100-μm cover glass. Results are shown for the different perovskite layers.

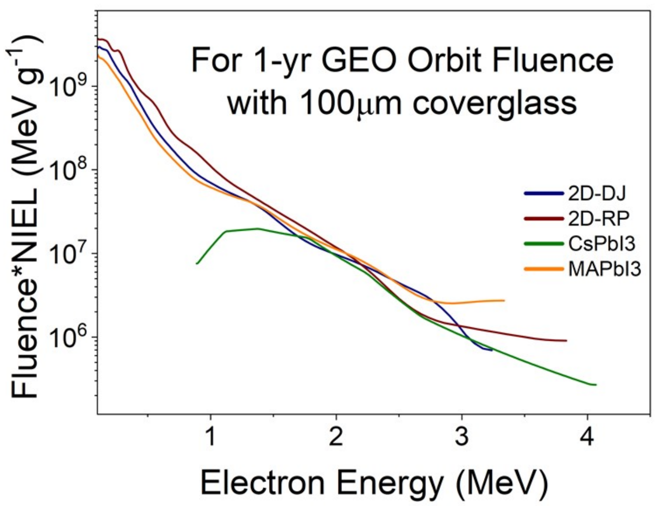

Figure S11. Displacement damage dose (DDD) versus electron energy for the GEO orbit, computed from one-year electron fluence, with a 100-μm cover glass. Results are shown for the different perovskite layers.

Table S1. Interface parameters of all-2D PSC.

Parameters/Interfaces	$MoS_2/(ThMA)_2(MA)_2Pb_3I_{10}$	$(ThMA)_2(MA)_2Pb_3I_{10}$/graphene
Defect type	Neutral	Neutral
Capture cross section for electrons (cm^2)	1×10^{-19}	1×10^{-19}
Capture cross section for holes (cm^2)	1×10^{-19}	1×10^{-19}
Energetic Distribution	Single	single
Reference for defect energy level E_t	Above the highest E_V	Above the highest E_V
Energy with respect to reference (eV)	0.600	0.600
Total density ($1/cm^2$)	1.05×10^{13}	1.0×10^{10}

Table S2: Photovoltaic parameters of all-2D PSCs before and after optimization.

Device	V_{OC} (V)	J_{SC} (mA/cm^2)	FF (%)	PCE (%)
Before optimization	1.25	15.15	37.23	5.22
After optimization	1.39	29.36	76.65	23.04

Table S3. The literature-based parameters of the layers utilized in PSC simulation.

Parameters	$MAPbI_3$	$CsPbI_3$	$(BDA)MA_2Pb_3I_{10}$	c-Si (n)	c-Si (p)	c-Si (p^+)
Thickness (nm)	600	600	600	100	10000	30
E_g (eV)	1.55	1.68	1.64	1.124	1.124	1.124
χ_e (eV)	3.9	3.55	3.8	3.9	4.05	3.9
ε_r	25	6	25	11.9	11.9	11.9
N_C (cm^{-3})	2.2×10^{18}	2.2×10^{18}	2.2×10^{18}	2.8×10^{19}	2.8×10^{19}	2.8×10^{19}
N_V (cm^{-3})	1.8×10^{19}	1.8×10^{19}	1.8×10^{19}	1.04×10^{19}	1.04×10^{19}	1.04×10^{19}
μ_e ($cm^2 V^{-1} s^{-1}$)	25	25	3.10×10^{-4}	1260	1010	1212
μ_h ($cm^2 V^{-1} s^{-1}$)	105	25	6.30×10^{-4}	443	443	421
N_D (cm^{-3})	---	---	---	8.0×10^{19}	---	---
N_A (cm^{-3})	1.0×10^{16}	1.0×10^{16}	1.0×10^{16}	---	5.0×10^{15}	9.0×10^{18}
N_T (cm^{-3})	1.0×10^{14}	1.0×10^{14}	1.0×10^{14}	1.0×10^{12}	1.0×10^{12}	1.0×10^{12}
References	[1, 2]	[3, 4]	[5]	[6, 7]	[6, 7]	[6, 7]

Table S4: Average number of vacancies produced per ion within different device structures under varying proton energies.

Device/Energy	0.05 MeV	0.1 MeV	0.5 MeV	1.0 MeV
2D-RP	9.25	12.45	1.03	0.51
2D-DJ	9.30	12.49	0.94	0.51
$CsPbI_3$	7.10	10.40	1.65	0.70
$MAPbI_3$	8.73	12.50	1.09	0.68
Tandem	16.11	18.33	28.70	8.85

Table S5: Summary of selected literature studies on proton-irradiated perovskite photovoltaics under AM0 illumination, compared with the present simulated all-2D layered PSC structure (FTO/MoS_2/$(ThMA)_2(MA)_2Pb_3I_{10}$/Graphene/Au).

Structure	V_{OC} (V)	J_{SC} (mA cm^{-2})	FF (%)	PCE (%)	Year	Ref.
ITO/TiO_2/$FAPbI_3$/spiro-OMeTAD/Ag	0.99	17.70	70.00	12.50	2017	[8]
ITO/PEDOT:PSS/$MAPbI_3$/$PC_{61}BM$/BCB/Ag	0.96	8.70	69.00	5.76	2017	[9]
ITO/SnO_2/ $(FA_{0.79}MA_{0.16}Cs_{0.05})_{0.97}Pb(I_{0.84}Br_{0.16})_{2.97}$/spiro-OMeTAD/$MoO_x$/Al	1.01	10.09	72.07	12.57	2018	[10]
ITO/TiO_2/$MAPbI_3$/P3HT/Au	0.66	12.50	75.00	4.80	2018	[11]
AZO/SnO_2/Cs(MAFA)$Pb(IBr)_3$/spiro-OMeTAD/Au	1.11	26.60	62.80	13.60	2019	[12]
ITO/PTAA/Cs(MAFA)$Pb(IBr)_3$/C_{60}/BCP/Cu	1.12	23.22	70.00	18.20	2019	[13]
LiF/IZO/SnO_2/C_{60}/Perovskite/PTAA/NiO_x/ZnO/CdS/CIGS/Mo	1.55	20.00	65.70	15.20	2020	[14]
ITO/polyTPD/PFN-Br/$FA_{0.8}Cs_{0.2}Pb(IBrCl)_3$/LiF/$C_{60}$/SnOx/ZTO/ITO	1.03	16.24	71.50	8.88	2021	[15]
ITO/PEDOT:PSS/PTFE/$(FASn)_{0.6}(MAPb)_{0.4}I_3$/$PC_{61}BM$/$C_{60}$/TmPyPB/Ag	0.77	27.44	68.80	10.77	2021	[16]
FTO/TiO_2/$MAPbI_3$/spiro-OMeTAD/Au	0.92	14.65	53.08	7.20	2022	[17]
FTO/TiO_2/$Cs_{0.01}MA_{0.01}FA_{0.98}PbI_3$/spiro-OMeTAD/Au	---	---	---	13.96	2023	[18]
ITO/SnO_2/Cs (MA)(FA)$Pb(IBr)_3$/spiro-OMeTAD/Au	1.07	21.67	65.00	15.13	2023	[19]
ITO/PEDOT:PSS/$Cs_{0.05}FA_{0.80}MA_{0.15}Pb(IBr)_3$/PCBM/PEIE/Au	0.95	20.20	59.80	11.60	2024	[20]
FTO/SnO_2/$Cs_{0.04}Rb_{0.04}(F_{A0.65}MA_{0.35})_{0.92}Pb(I_{0.85}Br_{0.14}Cl_{0.01})_3$/spiro-OMeTAD/Au	1.13	21.95	59.00	14.75	2024	[21]
ITO/Me-4PACz/Al_2O_3/$(Cs_{0.22}FA_{0.78})Pb(I_{0.79}Br_{0.17}Cl_{0.04})_3$/$PDAI_2$/$C_{60}$/$SnO_2$/Ag	1.14	19.10	70	15.04	2025	[22]
FTO/SnO_2/Cs(MAFA)PbI_3/spiro-OMeTAD/Au	0.94	19.27	56.00	10.24	2025	[23]
FTO/MoS_2/$(ThMA)_2(MA)_2Pb_3I_{10}$/Graphene/Au	**1.38**	**29.40**	**79.05**	**23.70***	**2025**	**This work**
	1.32	**28.37**	**59.07**	**16.33#**		

* The PSC performance in ISS orbit with using 5-μm glass shielding.

\# The PSC performance in GEO orbit with using 5-μm glass shielding.

References

[1] S. Govinda, B.P. Kore, M. Bokdam, P. Mahale, A. Kumar, S. Pal, B. Bhattacharyya, J. Lahnsteiner, G. Kresse, C. Franchini, Behavior of methylammonium dipoles in MAPbX3 (X= Br and I), The journal of physical chemistry letters 8(17) (2017) 4113-4121.
[2] Q. Dong, Y. Fang, Y. Shao, P. Mulligan, J. Qiu, L. Cao, J. Huang, Electron-hole diffusion lengths> 175 μm in solution-grown CH3NH3PbI3 single crystals, Science 347(6225) (2015) 967-970.
[3] X. Liu, J. Zhang, H. Wang, Y. Miao, T. Guo, L.K. Ono, S. Yuan, Y. Wang, P. Ji, H. Chen, CsPbI3 perovskite solar module with certified aperture area efficiency> 18% based on ambient-moisture-assisted surface hydrolysis, Joule 8(10) (2024) 2851-2862.
[4] J. Yuan, D. Zhang, B. Deng, J. Du, W.C. Choy, J. Tian, High efficiency inorganic perovskite solar cells based on low trap density and high carrier mobility CsPbI3 films, Advanced Functional Materials 32(47) (2022) 2209070.
[5] Y. Zheng, T. Niu, J. Qiu, L. Chao, B. Li, Y. Yang, Q. Li, C. Lin, X. Gao, C. Zhang, Oriented and uniform distribution of Dion–Jacobson phase perovskites controlled by quantum well barrier thickness, Solar Rrl 3(9) (2019) 1900090.
[6] K. Yoshikawa, H. Kawasaki, W. Yoshida, T. Irie, K. Konishi, K. Nakano, T. Uto, D. Adachi, M. Kanematsu, H. Uzu, Silicon heterojunction solar cell with interdigitated back contacts for a photoconversion efficiency over 26%, Nature energy 2(5) (2017) 1-8.
[7] E. Akoto, V. Isahi, V. Odari, C. Maghanga, F. Nyongesa, Monolith Cs1-xRbxSnI3 perovskite–silicon 2T tandem solar cell using SCAPS-1D, Results in Optics 12 (2023) 100470.
[8] J.S. Huang, M.D. Kelzenberg, P. Espinet-González, C. Mann, D. Walker, A. Naqavi, N. Vaidya, E. Warmann, H.A. Atwater, Effects of Electron and Proton Radiation on Perovskite Solar Cells for Space Solar Power Application, 2017 IEEE 44th Photovoltaic Specialist Conference (PVSC), 2017, pp. 1248-1252.
[9] V.V. Brus, F. Lang, J. Bundesmann, S. Seidel, A. Denker, B. Rech, G. Landi, H.C. Neitzert, J. Rappich, N.H. Nickel, Defect dynamics in proton irradiated CH3NH3PbI3 perovskite solar cells, Advanced Electronic Materials 3(2) (2017) 1600438.
[10] C. Brown, G. Eperon, V. Whiteside, I. Sellers, Potential of high-stability perovskite solar cells for low-intensity–low-temperature (LILT) outer planetary space missions, ACS Applied Energy Materials 2(1) (2018) 814-821.
[11] Y. Miyazawa, M. Ikegami, H.-W. Chen, T. Ohshima, M. Imaizumi, K. Hirose, T. Miyasaka, Tolerance of Perovskite Solar Cell to High-Energy Particle Irradiations in Space Environment, iScience 2 (2018) 148-155.
[12] J. Barbé, D. Hughes, Z. Wei, A. Pockett, H.K. Lee, K.C. Heasman, M.J. Carnie, T.M. Watson, W.C. Tsoi, Radiation hardness of perovskite solar cells based on aluminum-doped zinc oxide electrode under proton irradiation, Solar RRL 3(12) (2019) 1900219.
[13] F. Lang, M. Jošt, J. Bundesmann, A. Denker, S. Albrecht, G. Landi, H.-C. Neitzert, J. Rappich, N.H. Nickel, Efficient minority carrier detrapping mediating the radiation hardness of triple-cation perovskite solar cells under proton irradiation, Energy & Environmental Science 12(5) (2019) 1634-1647.
[14] F. Lang, M. Jošt, K. Frohna, E. Köhnen, A. Al-Ashouri, A.R. Bowman, T. Bertram, A.B. Morales-Vilches, D. Koushik, E.M. Tennyson, Proton radiation hardness of perovskite tandem photovoltaics, Joule 4(5) (2020) 1054-1069.
[15] B.K. Durant, H. Afshari, S. Singh, B. Rout, G.E. Eperon, I.R. Sellers, Tolerance of perovskite solar cells to targeted proton irradiation and electronic ionization induced healing, ACS Energy Letters 6(7) (2021) 2362-2368.
[16] B.K. Durant, H. Afshari, S. Sourabh, V. Yeddu, M.T. Bamidele, S. Singh, B. Rout, G.E. Eperon, D.Y. Kim, I.R. Sellers, Radiation stability of mixed tin–lead halide perovskites: Implications for space applications, Solar Energy Materials and Solar Cells 230 (2021) 111232.
[17] W.O.H. Martínez, N.B.C. Guerrero, V.A.G. Andrade, M. Alurralde, M.D. Perez, Evaluation of the resistance of halide perovskite solar cells to high energy proton irradiation for space applications, Solar Energy Materials and Solar Cells 238 (2022) 111644.

[18] N. Liu, L. Zhang, Y. Liang, B. Xue, D. Wang, Effects of carrier transport layers on performance degradation in perovskite solar cells under proton irradiation, ACS Applied Energy Materials 6(12) (2023) 6673-6680.

[19] A.R. Kirmani, D.P. Ostrowski, K.T. VanSant, T.A. Byers, R.C. Bramante, K.N. Heinselman, J. Tong, B. Stevens, W. Nemeth, K. Zhu, Metal oxide barrier layers for terrestrial and space perovskite photovoltaics, Nature Energy 8(2) (2023) 191-202.

[20] D. Angmo, S. Yan, D. Liang, A.D. Scully, A.S.R. Chesman, M. Kellam, N.W. Duffy, N. Carter, R. Chantler, C. Chen, M. Gao, Toward Rollable Printed Perovskite Solar Cells for Deployment in Low-Earth Orbit Space Applications, ACS Applied Energy Materials 7(5) (2024) 1777-1791.

[21] H.P. Parkhomenko, M.M. Solovan, S. Sahare, A.I. Mostovyi, D. Aidarkhanov, N. Schopp, T. Kovaliuk, M. Kaikanov, A. Ng, V.V. Brus, Impact of a short-pulse high-intense proton irradiation on high-performance perovskite solar cells, Advanced Functional Materials 34(10) (2024) 2310404.

[22] H. Shim, S. Seo, C. Chandler, M.K. Sharpe, C.D. McAleese, J. Lim, B.-S. Kim, S. Roy, I. Jayawardena, S.R.P. Silva, Enhancing radiation resilience of wide-band-gap perovskite solar cells for space applications via A-site cation stabilization with PDAI2, Joule 9(8) (2025).

[23] B. Xue, L. Zhang, T. Zhang, N. Liu, A. Ejaz, Y. Liang, Degradation behavior and damage mechanisms of perovskite solar cells under 50–200 keV proton irradiations, Solar Energy Materials and Solar Cells 282 (2025) 113442.